A Maximum Entropy Analysis of Protein Orientations Using Fluorescence Polarization Data from Multiple Probes

Uulke A. van der Heide, Seth C. Hopkins, and Yale E. Goldman
Pennsylvania Muscle Institute, D701 Richards Building, The School of Medicine, University of Pennsylvania, Philadelphia, Pennsylvania 19104-6083, U.S.A.

ABSTRACT Techniques have recently become available to label protein subunits with fluorescent probes at predetermined orientation relative to the protein coordinates. The known local orientation enables quantitative interpretation of fluorescence polarization experiments in terms of orientation and motions of the protein within a larger macromolecular assembly. Combining data obtained from probes placed at several distinct orientations relative to the protein structure reveals functionally relevant information about the axial and azimuthal orientation of the labeled protein segment relative to its surroundings. Here we present an analytical method to determine the protein orientational distribution from such data. The method produces the broadest distribution compatible with the data by maximizing its informational entropy. The key advantages of this approach are that no a priori assumptions are required about the shape of the distribution and that a unique, exact fit to the data is obtained. The relative orientations of the probes used for the experiments have great influence on information content of the maximum entropy distribution. Therefore, the choice of probe orientations is crucial. In particular, the probes must access independent aspects of the protein orientation, and two-fold rotational symmetries must be avoided. For a set of probes, a "figure of merit" is proposed, based on the independence among the probe orientations. With simulated fluorescence polarization data, we tested the capacity of maximum entropy analysis to recover specific protein orientational distributions and found that it is capable of recovering orientational distributions with one and two peaks. The similarity between the maximum entropy distribution and the test distribution improves gradually as the number of independent probe orientations increases. As a practical example, ME distributions were determined with experimental data from muscle fibers labeled with bifunctional rhodamine at known orientations with respect to the myosin regulatory light chain (RLC). These distributions show a complex relationship between the axial orientation of the RLC relative to the fiber axis and the azimuthal orientation of the RLC about its own axis. Maximum entropy analysis reveals limitations in available experimental data and supports the design of further probe angles to resolve details of the orientational distribution.

INTRODUCTION

The functional output of many biological systems depends on rotations or orientational changes of protein components within a macromolecular framework (Polekhina et al., 1996; Yasuda et al., 1998; Zhang et al., 1998; Dominguez et al., 1998). A technique commonly used to characterize orientational distributions and rotational dynamics is fluorescence polarization of a probe molecule bound to the protein subunit (Weber, 1952; Lakowicz, 1983). An example is the study of muscle contraction, where functionally relevant orientation changes of myosin cross-bridges have been detected using bound extrinsic fluorescent probes (Irving et al., 1995; Hopkins et al., 1998; Corrie et al., 1999).

Although it is relatively straightforward to directly interpret the fluorescence polarization data in terms of probe angular changes, quantifying the underlying orientational distribution of the labeled proteins themselves requires knowledge of the orientation of the probe relative to the protein. Methods to estimate the local orientations of spectroscopic probes involve assumptions about the hydrodynamic properties of the proteins (Burghardt and Ajtai, 1994) or prior knowledge of their orientation in a macromolecular system (Fajer, 1994).

These issues were addressed in a recent study of the orientational distribution of the myosin regulatory light chain in muscle fibers (Sabido-David et al., 1997; Hopkins et al., 1997; Corrie et al., 1999). Bis-(iodoacetamido)-tetramethylrhodamine (Corrie et al., 1998) was covalently attached to two appropriately spaced cysteine residues engineered into the light chain amino acid sequence. With this arrangement, the average orientation of the probe absorption and emission dipoles is along a line joining the two cysteines (Ferguson et al., 1997). Several such bifunctionally labeled mutants, giving various probe orientations relative to the light chain, were used to determine the axial (tilt) angle of the protein relative to the fiber and the azimuthal (twist) angle around the protein axis.

The information about orientational order obtained in fluorescence polarization experiments is typically limited to the second- and fourth-rank order parameters of the probe molecule distribution relative to the sample director (e.g., the fiber axis or membrane normal, Zannoni et al., 1983), although other information may be accessible using nonstandard fluorescence techniques (Burghardt and Ajtai, 1994; Bell et al., 2000). The data are conventionally interpreted by postulating a model for the shape of the orienta-

Received for publication 17 May 1999 and in final form 16 December 1999.

Address reprint requests to Yale E. Goldman, Pennsylvania Muscle Institute, D701 Richards Building, The School of Medicine, University of Pennsylvania, Philadelphia, Pennsylvania 19104-6083. Tel.: 215-898-4017; Fax: 215-898-2653; E-mail: goldmany@mail.med.upenn.edu.

0006-3495/00/04/2138/13 $2.00

tional distribution and fitting it to these order parameters or to the polarized fluorescence intensities. Some examples are a helical distribution plus a randomly oriented component, a Gaussian distribution and a wobble in a cone (Kinosita et al., 1977; Wilson and Mendelson, 1983; Hopkins et al., 1998). This approach provides insight into the orientation and axial motions, but the information is limited by the choice of model distribution. Furthermore, the conclusions may depend on the specific model chosen (e.g., Berger et al., 1996).

Such models for the distribution of axial angles can be generalized quite easily to accommodate both the protein axial and azimuthal angles. A drawback, however, is that these types of models may not describe the underlying orientational distribution very accurately. This problem results in differences between predicted and observed order parameters that may be larger than expected based on the uncertainties in the data (e.g., Fig. 2 in Corrie et al., 1999).

Here we take an approach that avoids a priori assumptions about the shape of the orientational distribution by calculating it directly from the data. We obtain the broadest orientational distribution for the protein consistent with the data by maximizing the entropy of the distribution. Maximum entropy (ME) analysis has been used before to describe the axial distribution of cylindrically symmetric probes in lipid bilayers (Kooyman et al., 1983; Zannoni, 1988), but not in regard to multiple probes at distinct relative orientations. The rationale for maximizing the entropy is the mathematical identification of thermodynamic entropy with the degree of uncertainty about the system (Shannon, 1948; Jaynes, 1957; Levine and Tribus, 1979). An additional advantage of the approach is that the maximum entropy analysis accommodates all possible physical combinations of measured order parameters. The ME distribution fits data from several fluorescent probes exactly without requiring additional information. The exact fit implies that no information is lost from the original order parameter data and that those data can be recovered exactly from the ME distribution for any other type of analysis. Although we emphasize bifunctional fluorescent probes, the analysis is also applicable to other systems where data are available from multiple spectroscopic probes at known orientations (e.g., Ajtai et al., 1994).

In this paper, we present a practical guideline to maximum entropy analysis of data from multiple probes. We derive the general form of the ME distribution for an arbitrary number of probes and show that the relative orientations of the probes affect the information that can be retrieved about the protein orientational distribution. In planning the experiment, therefore, care is required in the choice of labeling sites. In an Appendix, we discuss quantitative measures for the selection of probe orientations. In Results, we present a group of simulations that show the capability of ME analysis to recover specific test distributions including distributions with multiple peaks. ME distributions from experimental data on muscle fibers are calculated as an example application. The analysis shows that the ME distribution reveals the likely orientation of the protein and also the limitations and ambiguities of the experimental data on which it is based. Part of this work has previously been presented in abstract form (Van der Heide et al., 1998).

THEORY

Fluorescence polarization

Consider a protein in a cylindrically symmetric, ordered system. A fluorescent probe molecule, with colinear absorption and emission dipole moments, is attached at a known orientation relative to the protein. In xanthene derivative fluorophores, such as rhodamine and eosin, the absorption and emission dipoles lie nearly parallel (Chen and Bowman, 1965; VanderMeulen et al., 1990; Van der Heide et al., 1992) and the approximation of colinearity is justified. In a fluorescence polarization experiment, intensity ratios are obtained that provide information on the orientational order and rotational dynamics of the transition dipole moments in the system (Lakowicz, 1983; Zannoni et al., 1983; Kooyman et al., 1983). After factoring out depolarization due to fast wobble of the probe (Dale et al., 1999), the intensity ratios provide information about the probe orientational distribution in terms of the order parameters, $\langle P_2 \rangle$ and $\langle P_4 \rangle$, defined as

$$\langle P_L \rangle_d = \int_0^\pi g_d(\beta_{fd}) P_L(\cos \beta_{fd}) \sin \beta_{fd} \, d\beta_{fd}, \qquad (1)$$

where $g_d(\beta_{fd})$ is the orientational distribution of the probe dipole moment relative to the fiber axis (Zannoni, 1988), $P_L(z)$ is the Lth Legendre polynomial, e.g., $P_2(z) = (3z^2 - 1)/2$, $P_4(z) = (35z^4 - 30z^2 + 3)/8$, and β_{fd} is the axial angle between probe transition dipole **d** and the sample director (muscle fiber axis) **f** (see Fig. 1). The order parameters represent the second- and fourth-rank Legendre polynomials averaged over the distribution of orientations of **d** relative to **f**. $g_d(\beta_{fd})$ is normalized according to $\int_0^\pi g_d(\beta_{fd}) \sin \beta_{fd} \, d\beta_{fd} = 1$.

These order parameters can also be expressed in terms of the protein orientation and the orientation of the probe transition dipole relative to the protein. A coordinate frame in the protein is defined by three axes $\mathbf{p}_x$, $\mathbf{p}_y$, and $\mathbf{p}_z$ (Fig. 1). The axial angle of the protein, β_{fp}, is the angle between $\mathbf{p}_z$ and the director **f**. The azimuthal (twist) angle of the protein around $\mathbf{p}_z$ is given by γ_{fp} and is defined to be zero when the axis $\mathbf{p}_x$ lies in the plane of **f** and $\mathbf{p}_z$ and the projection of $\mathbf{p}_x$ on **f** is negative. The vector $\mathbf{p}_0$ in Fig. 1 defines the position of $\mathbf{p}_x$ when $\gamma_{fp} = 0$. An increase in γ_{fp} corresponds to a counter-clockwise rotation when looking toward **f**. The ax-

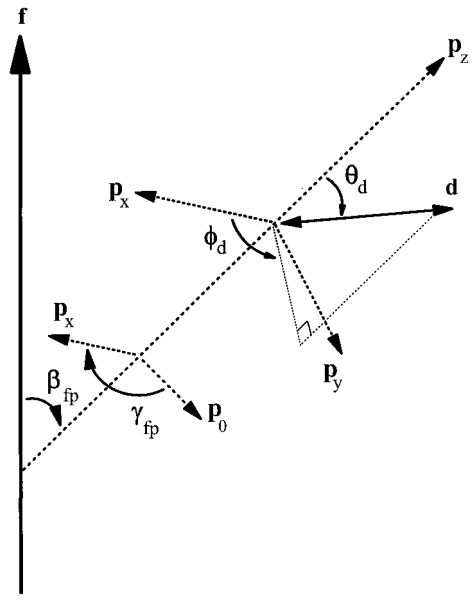

FIGURE 1 Geometrical relationship between the sample axis (**f**), the protein frame ($\mathbf{p}_x$, $\mathbf{p}_y$, $\mathbf{p}_z$), and the probe dipole (**d**). θ_d is the axial angle of **d** relative to $\mathbf{p}_z$. ϕ_d is the azimuthal angle of **d** around $\mathbf{p}_z$. β_{fp} is the axial angle of the protein relative to **f**. γ_{fp} is the azimuthal angle of the protein around the protein ($\mathbf{p}_z$) axis. The vector $\mathbf{p}_0$ defines the position of $\mathbf{p}_x$ when $\gamma_{fp} = 0$. $\mathbf{p}_0$ is perpendicular to $\mathbf{p}_z$, in the plane containing **f** and $\mathbf{p}_z$, and points away from **f**. An increase in γ_{fp} or ϕ_{pd} corresponds to a counter-clockwise rotation around $\mathbf{p}_z$, when looking from the protein toward the fiber axis. The values of ϕ_d and γ_{fp} shown correspond to approximately 70° (counter-clockwise from $\mathbf{p}_x$) and −130° (clockwise from $\mathbf{p}_0$). The angle β_{fd} mentioned in the text is the axial angle of **d** relative to **f**.

ial angle of **d** relative to the protein frame is given by θ_d, the azimuthal angle by ϕ_d (Fig. 1).

The completion theorem gives $\cos\beta_{fd}$ in terms of protein orientation and local dipole orientation

$$\cos\beta_{fd} = \cos\beta_{fp}\cos\theta_d - \sin\beta_{fp}\sin\theta_d\cos(\gamma_{fp} + \phi_d). \quad (2)$$

Then, the function required to calculate order parameters in terms of β_{fp} and γ_{fp} for a given dipole **d** is

$$P_{L,d}(\beta_{fp}, \gamma_{fp}) \equiv P_L(\cos\beta_{fd}) = P_L(\cos\beta_{fp}\cos\theta_d - \sin\beta_{fp}\sin\theta_d\cos(\gamma_{fp} + \phi_d)). \quad (3)$$

Define an orientational distribution of the protein relative to **f** as $f(\beta_{fp}, \gamma_{fp})$, normalized according to $\int_0^\pi\int_{-\pi}^{\pi} f(\beta_{fp}, \gamma_{fp})\, d\gamma_{fp} \sin\beta_{fp}\, d\beta_{fp} = 1$. The order parameters are obtained by integrating over this distribution

$$\langle P_L\rangle_d = \int_0^\pi\int_{-\pi}^{\pi} f(\beta_{fp}, \gamma_{fp}) P_{L,d}(\beta_{fp}, \gamma_{fp})\, d\gamma_{fp}\sin\beta_{fp}\, d\beta_{fp}. \quad (4)$$

From Eqs. 3 and 4, it is clear that, for a protein orientational distribution function $f(\beta_{fp}, \gamma_{fp})$, a set of several probes with distinct orientations, $\{\theta_1, \phi_1\}$, $\{\theta_2, \phi_2\}$, . . . , $\{\theta_n, \phi_n\}$, results in several sets of order parameters, $\{\langle P_2\rangle_1, \langle P_4\rangle_1\}$, $\{\langle P_2\rangle_2, \langle P_4\rangle_2\}$, . . . , $\{\langle P_2\rangle_n, \langle P_4\rangle_n\}$, one set for each probe. All of these order parameters, which can be determined experimentally, provide information about the orientational distribution of the protein.

Maximum entropy distributions

The entropy, S, of a distribution $f(\beta_{fp}, \gamma_{fp})$ is defined as

$$S\{f(\beta_{fp}, \gamma_{fp})\} = -\int_0^\pi\int_{-\pi}^{\pi} f(\beta_{fp}, \gamma_{fp})\ln\{f(\beta_{fp}, \gamma_{fp})\}\, d\gamma_{fp}\sin\beta_{fp}\, d\beta_{fp} \quad (5)$$

(Shannon, 1948; Jaynes, 1957; Levine and Tribus, 1979). The method of Lagrange multipliers (Mathews and Walker, 1970) can be used to derive the general form of $f(\beta_{fp}, \gamma_{fp})$ for which the entropy is maximized, subject to the constraints imposed by consistency with n pairs of order parameters and the requirement that $f(\beta_{fp}, \gamma_{fp})$ be normalized. A derivation is given in Appendix A. The so-called maximum entropy distribution is given by

$$f_{ME}(\beta_{fp}, \gamma_{fp}) = \exp\left\{-\lambda_0 - \sum_{d=1}^{n}(\lambda_{2,d}P_{2,d}(\beta_{fp}, \gamma_{fp}) + \lambda_{4,d}P_{4,d}(\beta_{fp}, \gamma_{fp}))\right\}, \quad (6)$$

where the $\lambda_{L,d}$ are constants, termed Lagrange multipliers, that govern the shape and height of the distribution and are determined by the constraints as explained below. The corresponding order parameters are calculated by inserting Eq. 6 into Eq. 4. For a single probe at orientation $\theta_d = 0$, this form reduces to the distribution used by Levine and coworkers (Kooyman et al., 1983). Given a set of experimentally obtained order parameters from n probes, the corresponding maximum entropy distribution can be found by adjusting the values of the $\lambda_{L,d}$ parameters until Eqs. 4 and 6 fit the order parameters. For a set of $2n$ independent constraints from n probes, there is a unique set of $2n$ values, $\lambda_{2,d}$, $\lambda_{4,d}$, . . . , defining the distribution function. λ_0 is a constant used for normalization.

In practice, a set of data will have an experimental uncertainty associated with it, represented by $\Delta\langle P_2\rangle_1$, $\Delta\langle P_4\rangle_1$, . . . , $\Delta\langle P_2\rangle_n$, $\Delta\langle P_4\rangle_n$. This will lead to an uncertainty, $\Delta\lambda_{L,d}$, in the corresponding Lagrange parameters as well. Because a direct interpretation of the Lagrange multipliers is cumbersome, an alternative is to calculate the corresponding uncertainty in the value of $f_{ME}(\beta_{fp}, \gamma_{fp})$ for

each point β_{fp}, γ_{fp} independently as

$$\frac{\Delta f_{ME}(\beta_{fp}, \gamma_{fp})}{f_{ME}(\beta_{fp}, \gamma_{fp})} = \left\{ (\Delta\lambda_0)^2 + \sum_{d=1}^{n} [(\Delta\lambda_{2,d} P_{2,d}(\beta_{fp}, \gamma_{fp}))^2 + (\Delta\lambda_{4,d} P_{4,d}(\beta_{fp}, \gamma_{fp}))^2] \right\}^{1/2}. \quad (7)$$

Choice of probe orientations

The sensitivity of fluorescence polarization to changes of protein orientation depends on the orientation of the probe relative to the rotation axis of the protein. Because a single probe may have an unfavorable orientation relative to the axis of rotation, at least two probe orientations are required to obtain quantitative information about rotational motions. A set of two probes is sensitive to both the azimuthal and axial rotations of the protein, but, due to the symmetry about the plane of the two probes, a clockwise azimuthal rotation cannot be distinguished from a counter-clockwise one. A third probe is required to resolve this ambiguity. Additional probes will refine the information about the orientational distribution of the protein in the system.

Because some combinations of probe orientations provide more information than others, the question arises as to how to select the best orientations for a set of probes. It should be recognized that this choice is affected foremost by the accessible attachment points. Binding sites must be available, or need to be engineered at positions that allow labeling without compromising the protein's function. Apart from this requirement, there are two criteria for selecting probe orientations to maximize the amount of information they provide. First, the probe orientations must be sufficiently different to yield polarization ratios that are significantly distinct given the experimental errors. Second, the set of probes should avoid mirror and rotational symmetries. For example, two probes at perpendicular orientations exhibit an 8-fold symmetry (2-fold around both probe axes and 2-fold about the axis perpendicular to both probes). Due to these symmetries, the protein could be oriented in any of eight orientations and give identical polarization ratios. The symmetry is reduced to a 4-fold ambiguity if the probes are not perpendicular (see Results).

The strategy is now to find n probe orientations that are as mutually exclusive as possible to provide the maximum independent information. Toward this goal, a "figure of merit," M, for the mutual independence among probes, is proposed in Appendix B. For a set of completely independent probes $M = 1$; for a set of identical probes $M = 0$. The figure of merit takes into account both the difference between probe orientations to give significantly different polarization ratios and considerations for avoiding ambiguity due to symmetries.

If we define the protein frame to be along the axis of the first probe ($\theta_1 = 0$), then, according to the figure of merit, the ideal second probe is at $\theta_2 = 54.7°$. If we define the x and y axes in the protein so that the azimuthal orientation of the second probe is $\phi_2 = 0$, then ideal position for a third probe is at $\theta_3 = 54.7°$ and $\phi_3 = 68.5°$, 137.1°, or 205.6°.

Note that the ideal relative orientations of the probes do not depend on the choice of protein frame. The azimuthal orientations enter the equations only as $\gamma_{fp} + \phi_d$, so only this sum is relevant rather than the absolute orientations. Orientations for further probes in a system are calculated as described in Appendix B. These choices are optimal if no prior knowledge is available about the specific protein orientation in the macromolecular frame of the sample. However, when information about the protein orientation is available, other choices may be more suitable.

RESULTS

Simulations

We tested the capacity of the ME analysis to recover specific protein orientational distributions in a series of simulations. We picked sets of up to five probe orientations θ_d, ϕ_d with respect to the protein, and calculated the order parameters $\langle P_2 \rangle_d$ and $\langle P_4 \rangle_d$ for a series of model protein distributions $f_{model}(\beta_{fp}, \gamma_{fp})$, where β_{fp} is the axial angle of the protein with respect to the sample director, and γ_{fp} is azimuthal (twist) angle of the protein around its own axis (Fig. 1). Then, we used the calculated order parameters to find the corresponding ME distribution, $f_{ME}(\beta_{fp}, \gamma_{fp})$ as described above. In practice, the order parameters would be determined in an experiment. Ideally $f_{ME}(\beta_{fp}, \gamma_{fp})$ should approximate $f_{model}(\beta_{fp}, \gamma_{fp})$. This ideal is approached gradually as the number of appropriately chosen probes increases.

The fluorescence polarization technique intrinsically exhibits a twofold symmetry, so that, for cylindrically symmetric systems, $f(\beta_{fp}, \gamma_{fp})$ cannot be distinguished from $f(180° - \beta_{fp}, 180° + \gamma_{fp})$. This ambiguity reflects the dipole character of the interaction of polarized light with the fluorescent probe. Therefore, we implicitly use a superposition of the two equivalent distributions throughout the remainder of this paper, i.e.,

$$f^*_{model}(\beta_{fp}, \gamma_{fp}) = \tfrac{1}{2} f_{model}(\beta_{fp}, \gamma_{fp}) + \tfrac{1}{2} f_{model}(180° - \beta_{fp}, 180° + \gamma_{fp}). \quad (8)$$

To compare $f_{ME}(\beta_{fp}, \gamma_{fp})$ with $f_{model}(\beta_{fp}, \gamma_{fp})$, a χ^2 figure is calculated as

$$\chi^2 = \int_0^{\pi} \int_{-\pi}^{\pi} \{f^*_{model}(\beta_{fp}, \gamma_{fp}) - f_{ME}(\beta_{fp}, \gamma_{fp})\}^2 \, d\gamma \sin\beta \, d\beta. \quad (9)$$

χ^2 is zero if $f_{ME}(\beta_{fp}, \gamma_{fp})$ and $f_{model}(\beta_{fp}, \gamma_{fp})$ are identical and increases as the correspondence worsens.

For $f_{model}(\beta_{fp}, \gamma_{fp})$, we first tested Gaussian distributions with a dispersion in both axial angle β_{fp} and azimuthal angle γ_{fp}. Subsequently, we tested the superposition of two nonequivalent Gaussian distributions to assess the capability of the maximum entropy analysis to resolve two populations.

Symmetries

The single Gaussian distribution for both the axial (β) and azimuthal (γ) orientations of the protein relative to the sample director **f** is defined as

$$f_{model}(\beta_{fp}, \gamma_{fp}) = \frac{1}{N}\exp\left\{-\frac{1}{2}\left(\frac{\beta_0 - \beta_{fp}}{\sigma_\beta}\right)^2 - \frac{1}{2}\left(\frac{\gamma_0 - \gamma_{fp}}{\sigma_\gamma}\right)^2\right\}, \quad (10)$$

where β_0, γ_0 defines the peak of the distribution, and σ_β and σ_γ the dispersions, N is a normalization constant. To emphasize the point made earlier about avoiding ambiguities due to symmetries in the selection of probe orientations, we first tested a set of probes at perpendicular angles relative to each other (Table 1, Set A). The model Gaussian distribution had parameters $\beta_0 = 50°$, $\gamma_0 = 50°$, $\sigma_\beta = 10°$, and $\sigma_\gamma = 20°$ (Fig. 2 *A*). Order parameters were calculated according to Eq. 4, and the ME map corresponding to the calculated order parameters was determined by fitting Eq. 6 to them. The corresponding ME maps for 1, 2, and 3 probes are shown in Fig. 2, *B–D*.

Data obtained from a single-probe dipole, oriented along the protein *z*-axis ($\theta_1 = 0°$, $\phi_1 = 0°$) are insensitive to the azimuthal angle γ_{fp} of the protein. Therefore, the reconstructed ME distribution shows a peaked distribution in only the axial direction (Fig. 2 *B*). Upon addition of data from a second probe at angles $\theta_2 = 90°$, $\phi_2 = 0°$, we recover a maximum entropy distribution with eight equivalent maxima (Fig. 2 *C*). Only two of these maxima correspond to the model distribution used as input. The other six arise from symmetries in the set of probe orientations that lead to identical polarization ratios if the protein is positioned in any of the eight corresponding orientations. Addition of a third probe perpendicular to the other two does not help to resolve this ambiguity at all (Fig. 2 *D*). The peaks themselves are somewhat sharper, but all eight peaks still have the same density.

TABLE 1 Probe angles relative to the protein frame

Probe Number	Axial Angle θ_{pd}	Azimuthal Angle ϕ_{pd}
	(degrees)	
Set A		
1	0	0
2	90	0
3	90	90
Set B		
1	0	0
2	54.7	0
3	54.7	137.1
4	54.7	68.5
5	54.7	205.6

A different picture emerges with the probes from Set B, which was designed to break the symmetries and optimize the information content following the procedure set out in Appendix B. The same Gaussian model distribution was used as input. Even with two probes, only four peaks with equal probabilities are found (Fig. 3 *A*). The mirror symmetry in the plane perpendicular to probe 1 is broken by the order parameters from the second probe, and, therefore, the ambiguity in the distribution between $f_{ME}(\beta_{fp}, \gamma_{fp})$ and $f_{ME}(180° - \beta_{fp}, \gamma_{fp})$ is removed. Adding a third probe further improves the correspondence (Fig. 3 *B*: compare to the test distribution in Fig. 2 *A*). Now, the mirror symmetry across the plane of probes 1 and 2 is also gone, which eliminates the ambiguity in the distribution between $f_{ME}(\beta_{fp}, \gamma_{fp})$ and $f_{ME}(\beta_{fp}, -\gamma_{fp})$. Only the two peaks in Fig. 3 *B* that reflect the intrinsic two-fold symmetry of the fluorescence polarization technique remain.

The simulations in Figs. 2 and 3 illustrate that the ME analysis reveals the information that is furnished by the data. If the data are ambiguous or consistent with multiple peaks, the ME distribution will reflect this uncertainty by showing them all superimposed. This does not mean that the actual physical distribution has multiple peaks, just that the available knowledge is insufficient to determine the real shape.

Data from more than three probes

The benefits of adding a fourth and a fifth probe orientation to the data set are mainly an improvement of the shape of the distribution. For the test model used for Figs. 2 and 3 and probe orientations chosen to optimize the information content (Table 1, Set B), the χ^2 value as defined in Eq. 9 is 0.034 for three probe orientations (cf., Fig. 3 *B*) and decreases to 0.002 for four probes and 0.001 for five (distributions not shown). These values indicate that the ME analysis recovers the starting model distribution very well.

We tested whether these results depend on the specific peak position and dispersions of the model distribution. With three probes, variation of the center of the peak, β_0 and γ_0, over its full range resulted in χ^2 values ranging from about 0.002 to 0.45. A better agreement was found for larger numbers of probe orientations. For four probes, χ^2 values were smaller than 0.05 in 90% of center positions. In the other 10% of center positions, we found χ^2 values as high as 0.25. For five probes, the χ^2 values were smaller than 0.025 over the full range of β_0 and γ_0.

The dispersion of the Gaussian model distribution was varied from $\sigma_\beta = 5°$, $\sigma_\gamma = 5°$ to $\sigma_\beta = 90°$, $\sigma_\gamma = 90°$ at a peak position of $\beta_0 = 50°$, $\gamma_0 = 50°$. The value of χ^2 for the

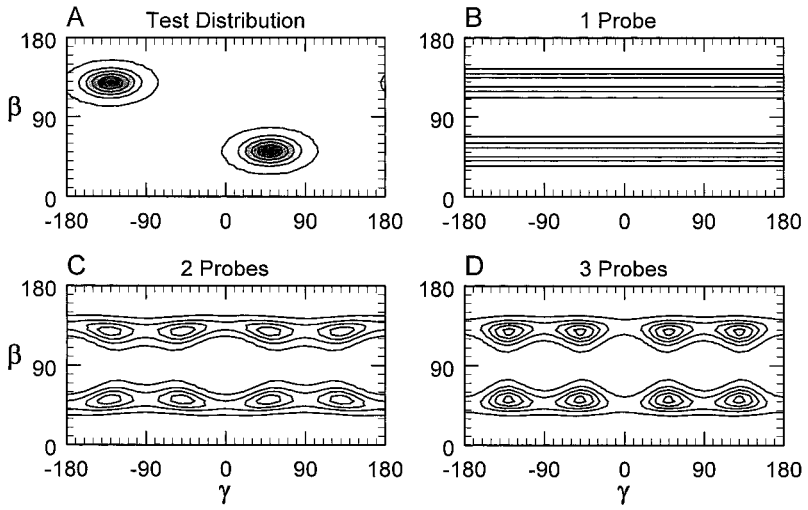

FIGURE 2 Contour plots of normalized model and ME number densities (distribution functions multiplied by sin β_{fp}). (*A*) Gaussian model distribution $\beta_0 = 50°$, $\gamma_0 = 50°$, $\sigma_\beta = 10°$, and $\sigma_\gamma = 20°$ (plus equivalent peak at $\beta_0 = 130°$, $\gamma_0 = -130°$). Maximum value $f_{max} = 1.33$. (*B*) ME number density for the first probe of set A in Table 1. $\chi^2 = 0.54$, $f_{max} = 0.20$. (*C*) ME map for probes 1–2 of set A. $\chi^2 = 0.51$, $f_{max} = 0.29$. (*D*) ME map for probes 1–3 of set A. $\chi^2 = 0.50$, $f_{max} = 0.34$. The range of the number density map runs from 0 (*white*) to 1.4 (*darkest gray*).

maximum entropy distributions obtained with three probes was smaller than 0.015 for $\sigma_\beta = \sigma_\gamma > 20°$. With four or five probes, χ^2 was smaller than 0.01 for σ_β and $\sigma_\gamma > 10°$. The ME distribution accommodates sharp distributions by assigning very high positive or negative values to some of the $\lambda_{k,d}$ parameters (cf., Eq. 6). For example, with $\beta_0 = 50°$, $\gamma_0 = 50°$, $\sigma_\beta = 10°$ and $\sigma_\gamma = 10°$, values of $\lambda_{k,d}$ in the range $+3.6$ to -15.7 appear in the exponent of Eq. 6. Calculations in this range are numerically demanding because a fine mesh is required for the integrations over the distribution (Eqs. 4 and 9). Experimental uncertainties would presumably limit the sharpness of the recovered distributions in such cases.

Distributions with two peaks

To study the ability of the maximum entropy analysis to recover distributions of different shapes, we tested a model distribution with two peaks. A double-peaked distribution was modeled by superimposing two Gaussian distributions of equal height (plus their two-fold rotational counterparts $f(180° - \beta_{fp}, 180° + \gamma_{fp})$), as shown in Fig. 4. The total distribution was normalized. The first peak is characterized by $\beta_0 = 30°$, $\gamma_0 = 0°$, $\sigma_\beta = 15°$, and $\sigma_\gamma = 30°$. The second peak is at $\beta_0 = 80°$, $\gamma_0 = 80°$, $\sigma_\beta = 20°$, and $\sigma_\gamma = 10°$. As shown in Fig. 4 *A*, the two peaks (and the two equivalent peaks at $\beta_0 = 150°$, $\gamma_0 = \pm 180°$ and $\beta_0 = 100°$, $\gamma_0 = -100°$) are well separated. Probe Set B was used again in this analysis.

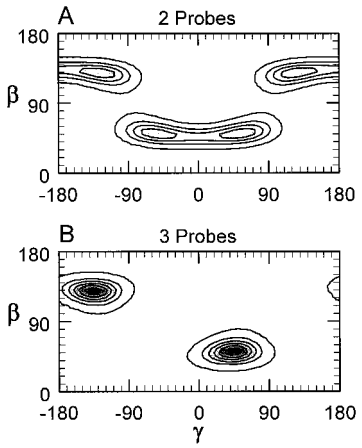

FIGURE 3 Contour plots of ME number densities corresponding to the test model shown in Fig. 2 *A*, but using probe set B in Table 1. (*A*) ME map for probes 1–2. $\chi^2 = 0.39$, $f_{max} = 0.49$. (*B*) ME map for probes 1–3. $\chi^2 = 0.06$, $f_{max} = 1.25$.

The ME distribution recovered from one probe again provides only information on the axial orientation. As shown above, a set of two probes gives information about the azimuthal angle γ_{fp}, but an ambiguity remains between $f_{ME}(\beta_{fp}, \gamma_{fp})$ and $f_{ME}(\beta_{fp}, -\gamma_{fp})$. Thus the peak at $\beta_{fp} = 80°$, $\gamma_{fp} = 80°$ in the model distribution is indistinguishable from $\beta_{fp} = 80°$, $\gamma_{fp} = -80°$, and that at $\beta_{fp} = 100°$, $\gamma_{fp} = -100°$ from $\beta_{fp} = 100°$, $\gamma_{fp} = 100°$. All these peaks contribute density to the ME distribution and overlap to some degree. As shown in Fig. 4 *C*, the maximum entropy distribution for 2 probes shows a hint of two peaks, but the distribution is symmetrical about $\beta_{fp} = 90°$ and $\gamma_{fp} = 0°$. At three probes (Fig. 4 *D*), the asymmetric nature of the original test distribution begins to emerge. The similarity to the input distribution (Fig. 4 *A*) improves with four and five probes (Fig. 4, *E* and *F*). However, the height of the peak at $\beta_{fp} = 30°$, $\gamma_{fp} = 0°$ is much greater relative to that at $\beta_{fp} = 80°$, $\gamma_{fp} = 80°$ than in the test distribution. Clearly, the two peaks of the distribution can be recognized, but the details of the distribution are not accurate.

Angular resolution

In this section, we test the angular resolution in more detail. We used model distributions that are a superposition of two

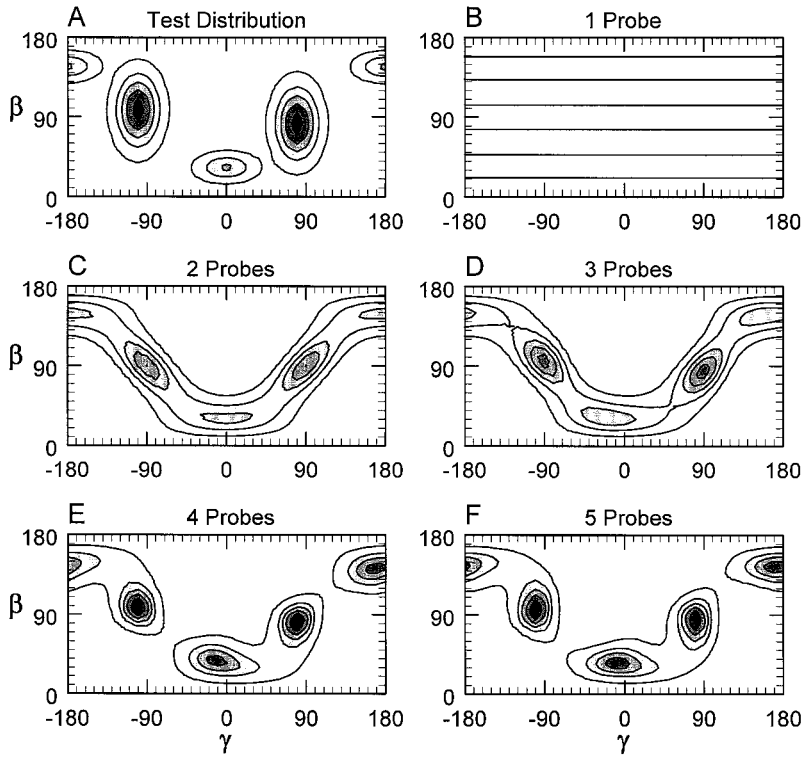

FIGURE 4 Contour plots of normalized model and ME number densities (distribution functions multiplied by sin β_{fp}). (*A*) Two-peaked Gaussian model distribution: first peak, $\beta_0 = 80°$, $\gamma_0 = 80°$, $\sigma_\beta = 20°$, and $\sigma_\gamma = 10°$ (plus equivalent symmetry-related peak); second peak, $\beta_0 = 30°$, $\gamma_0 = 0°$, $\sigma_\beta = 15°$, and $\sigma_\gamma = 30°$ (plus equivalent peak). Maximum value $f_{max} = 0.64$. (*B*) ME map for probe 1 of set B, Table 1. $\chi^2 = 0.19$, $f_{max} = 0.12$. (*C*) ME map for probes 1–2. $\chi^2 = 0.083$, $f_{max} = 0.45$. (*D*) ME map for probes 1–3. $\chi^2 = 0.075$, $f_{max} = 0.49$. (*E*) ME map for probes 1–4. $\chi^2 = 0.017$, $f_{max} = 0.72$. (*F*) ME map for probes 1–5. $\chi^2 = 0.009$, $f_{max} = 0.77$. The range of the number density map runs from 0 (*white*) to 0.61 (*darkest gray*).

populations, each with a Gaussian shape (Eq. 10) of equal height and width $\sigma = \sigma_\beta = \sigma_\gamma$. To test the resolution in the direction of β_{fp}, the center position of the first peak was set at $\beta_0 = 50°$, $\gamma_0 = 50°$. The center of the second peak was fixed at $\gamma_0 = 50°$, whereas β_0 was varied above 50° to separate the two peaks by an angle $\Delta\beta$. In Fig. 5, an example of a test model distribution and the maximum entropy solution are shown for a set of five probe orientations. $\Delta\beta$ between the two peaks is 45°, $\sigma = 20°$. A cross-section of the model distribution at $\gamma_{fp} = 50°$ shows that the two peaks are well resolved (Fig. 5 *B*). The maximum entropy solution recovered using the five probes of Set B is shown in Fig. 5 *C*, with the cross section in Fig. 5 *D*. Duplicity in the distribution is detectable although no minimum is found between the two maxima, indicating that the peaks are barely resolved (Sparrow's criterion; Smith, 1990). In Fig. 6 *A*, the angle $(\Delta\beta)_{res}$ at which the maximum entropy solution barely resolved the two peaks is plotted for simulations using 3, 4, and 5 probe orientations, and peak widths σ of 10–30°. The resolution is improved when more probes are added, because we find a smaller value $(\Delta\beta)_{res}$ with more mutants. An increase of $(\Delta\beta)_{res}$ with σ is caused simply by the fact that the starting model itself is barely resolved when the two peaks are separated by 2σ.

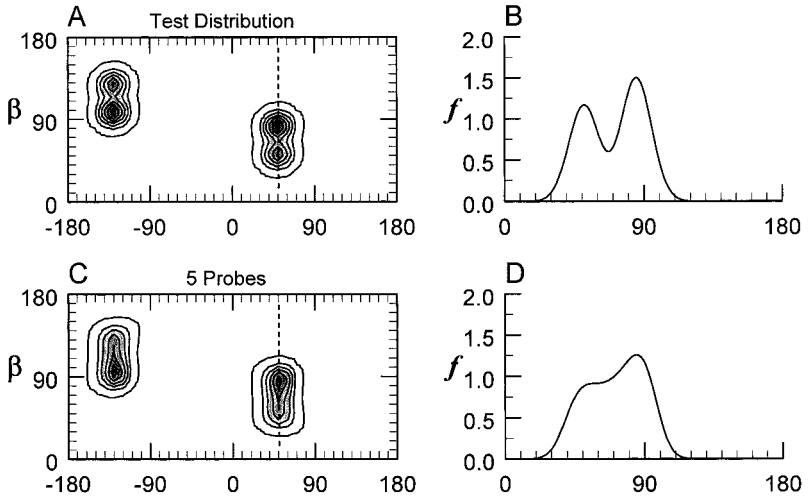

FIGURE 5 Contour plots of normalized model and ME number densities. (*A*) Two-peaked Gaussian model distribution. First peak, $\beta_0 = 50°$, $\gamma_0 = 50°$, $\sigma_\beta = 10°$, and $\sigma_\gamma = 10°$ (plus equivalent peak); second peak, $\beta_0 = 65°$, $\gamma_0 = 50°$, $\sigma_\beta = 10°$, and $\sigma_\gamma = 10°$ (plus equivalent peak). Maximum value $f_{max} = 1.50$. (*B*) Cross section through *A* at $\gamma_{fp} = 50°$. (*C*) ME map for probes 1–5 of set B, Table 1. $\chi^2 = 0.03$, $f_{max} = 1.25$. (*D*) Cross section through *B* at $\gamma_{fp} = 50°$. The range of the map runs from 0 (*white*) to 1.6 (*darkest gray*).

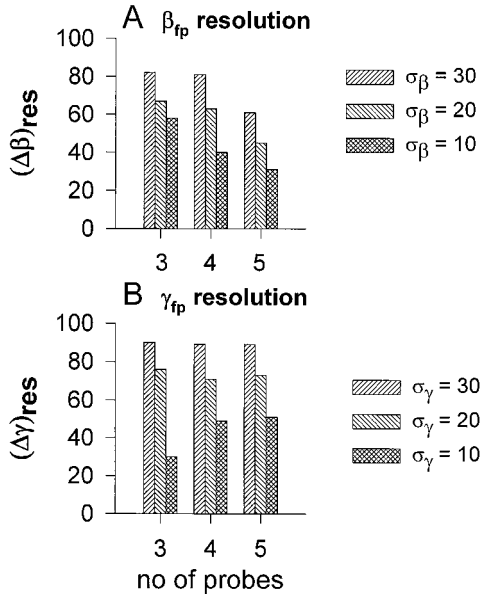

FIGURE 6. Minimum angular separation between two peaks that are resolved in ME distribution functions. (*A*) Minimum resolved $\Delta\beta_0$ for the first 3, 4, or 5 probes of set B, Table 1. (*B*) Minimum resolved $\Delta\gamma_0$ for the same 3, 4, or 5 probes.

Similarly, we tested the resolution in the direction of γ_{fp} by taking the center of the first peak as above, while fixing the second peak at $\beta_0 = 50°$ and $\gamma_0 = 50° + \Delta\gamma$. Fig. 6 *B* shows that $(\Delta\gamma)_{res}$ is worse than $(\Delta\beta)_{res}$ and does not improve upon increasing the number of probes for $\sigma = 20°$ or 30°. Surprisingly, for $\sigma = 10°$, the resolution is better for three probes than for four or five, but the positions of the two peaks are shifted to $\gamma_0 = 20°$ and 70°, indicating a poor correspondence to the starting model.

It must be noted that the correspondence of the maximum entropy distribution and the model distribution for some of these simulations is not very good (χ^2 up to 0.5). This deviation reflects the fact that the positions of the two peaks may be shifted and that their relative heights are not reproduced well. Thus, although the analysis is capable of recovering multiple populations, their positions and densities are not always accurate.

Example application

Corrie et al. (1999) presented steady-state and transient fluorescence polarization data from muscle fibers labeled with bifunctional rhodamine at known orientations with respect to the myosin regulatory light chain (RLC). The data from probes at four independent orientations were interpreted by fitting Gaussian distributions of the RLC orientation to the combined data. Fig. 7, *A* and *C* show maps of the RLC orientation corresponding to the Gaussian analysis of steady-state data during isometric activation and rigor. The ME distributions determined from the same data (panels *B* and *D*) show peaks in the approximately same overall positions. However, the ME distributions are not con-

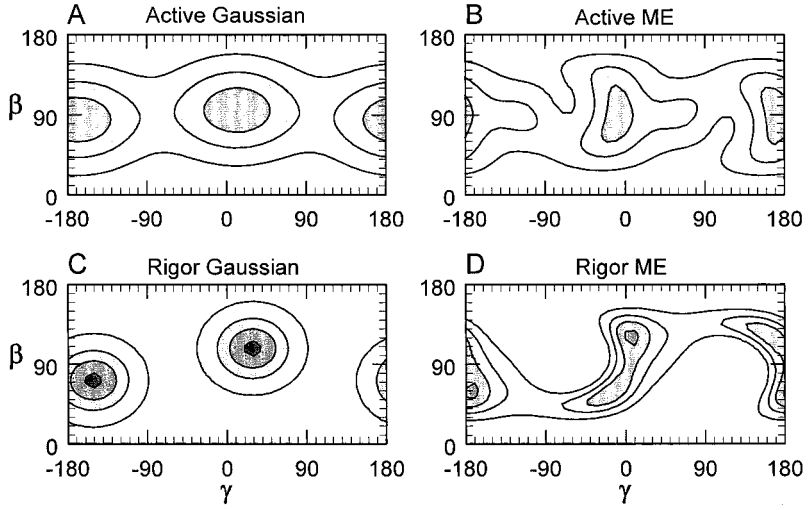

FIGURE 7. Analysis of data from four fluorescent probes labeling myosin RLC by Gaussian (*A* and *C*) and maximum entropy (*B* and *D*) distributions. The data are steady-state measurements during isometric activation and rigor (Corrie et al., 1999). Gaussian parameters β_0, σ_β, γ_0, and σ_γ defining the distributions are 96°, 37°, 12°, and 53°, respectively, in active contraction and 108°, 24°, 29°, and 29° in rigor (Corrie et al., 1999). Gaussian number densities (with sin β_{fp} weighting) were fit to the data in Corrie et al.; no additional sine weighting was applied in plotting panels *A* and *C*. For panels *B* and *D*, the polarization ratios shown in Fig. 2 of Corrie et al. (1999) were converted to probe order parameters (Dale et al., 1999), giving $\{\langle P_2\rangle, \langle P_4\rangle\}$ values of $\{-0.0260, -0.0254\}$, $\{0.0585, -0.0120\}$, $\{-0.0497, -0.0359\}$, and $\{-0.0609, -0.0136\}$ for 100-BR-108, 108-BR-113, 104-BR-115, and 100-BR-113 labeled RLC mutants, respectively, in active contraction and $\{-0.1166, -0.0457\}$, $\{-0.0488, -0.0731\}$, $\{-0.2335, -0.0083\}$, and $\{-0.2441, 0.0307\}$ in rigor. Maximum entropy distributions of the RLC orientation were calculated by fitting Eq. 6 to these order parameters and plotted as ME number densities (distribution functions multiplied by sin β_{fp}).

strained to an oval shape. Density in the ME maps, indicating likely orientations of the RLC, has a more complex relationship to β and γ.

The Gaussian analysis of Corrie et al. and the ME analysis in Fig. 7 used values for the probe orientations within the RLC corresponding to the line in the x-ray crystal structure joining the β-carbons of the two residues that were replaced by cysteines. This local orientation is given by θ_d and ϕ_d defined here in Fig. 1. To test the sensitivity of the calculated ME maps to these local angles, the maps were recalculated with θ_d and ϕ_d of each probe set 10° higher and lower than the values determined from the RLC crystal structure (with four probes, 16 maps were calculated for each condition). The effect was to shift the peaks of the ME distribution slightly, but the main features of the distribution, such as shape and separation of apparent domains, were robust. This behavior is presumably due to integration of information from all of the probes into the calculated maps.

DISCUSSION

Structural changes of proteins in larger assemblies can be monitored in real-time fluorescence polarization experiments using probes with known orientations relative to the protein coordinates (Hopkins et al., 1997; Corrie et al., 1999). Combining the data obtained from probes at distinct orientations relative to the protein reveals functionally relevant information about both the protein's axial and azimuthal orientation. Combining data from multiple probes has further advantages. A set of three nonperpendicular probes reduces the number of equally likely orientations for the protein from eight to two (cf., Figs. 2 and 3). In addition, data from multiple probes provide sufficient information to discriminate between various models for the protein orientational distribution.

In this paper, we show how to use maximum entropy analysis to derive a protein orientational distribution directly from the data without making a priori assumptions about the shape of the distribution. The method finds its rationale in the close relationship between two concepts of disorder, thermodynamic entropy, and informational entropy (Shannon, 1948; Jaynes, 1957). The experimental data provide information about the orientational distribution function, and thus reduce its entropy. The distribution that is consistent with the experimental data, but uses no additional information or assumptions about its shape, is the one that has the maximum entropy. Generally, it is the broadest distribution consistent with the data.

In the analysis of limited experimental data, there is often a trade-off between the complexity and realistic nature of a physical model. Models with more parameters can fit the data more accurately or exactly, but parsimony and limitations on the number and accuracy of the measured data points restrict the complexity. The method to achieve a balance between an accurate fit to the data and a realistic physical picture is called a regularization scheme (Press et al., 1992). Besides maximizing the entropy, there are other regularization criteria that can be used to obtain a protein orientational distribution consistent with the data. The degree of correspondence between the solution and the data can be weighed in various ways. Examples of alternative criteria are maximizing the smoothness of the distribution or the numerical stability of the solution (Press et al., 1992). The ME distribution fits data from several fluorescent probes exactly without requiring additional information. The exact fit implies that no information is lost from the original order parameter data and that those data can be recovered exactly from the ME distribution for any other type of analysis. The ME distribution has several further advantages already described above.

The issue of local probe orientation and combination of data from multiple probes has been taken up in previous studies. The orientation of probes relative to the protein coordinates has been assessed by molecular dynamics calculations (Mchaourab et al., 1996), spectroscopy of probes in proteins freely tumbling in solution (Ajtai et al., 1994), and static spectral measurements in a supramolecular system in which the protein orientation could be independently determined from earlier data (Fajer, 1994). Local orientations may also be adjustable variables in a global fit to spectroscopic data from multiple probes (Burghardt and Ajtai, 1992). Bifunctional probes bound to engineered residues confer the advantage that the local orientation is part of the experimental design, but the present analysis does not require this feature. The analysis presented here can be applied, however the axial and azimuthal angles of several probes are obtained relative to a defined coordinate frame in the protein.

When there is a reasonable expectation for characteristics of the orientational distribution in the system under study, it may be most practical to invoke a specific model to describe this distribution. In contrast, in many practical situations, it is not clear what to expect. Then, it becomes restrictive to consider only distributions of a particular shape, and a more suitable approach is the type of analysis presented here. A case that illustrates this point is the distribution with two populations shown in Fig. 4. A model that uses only a single peak would not fit the data. To describe such a distribution in terms of multiple populations of the Gaussian shape given in Eq. 10 requires four parameters for each peak plus relative weights among the peaks. When only six order parameters from three probe orientations are available, such a model is underdetermined. A simpler model could be constructed with fewer parameters, but extra assumptions would be required and it may not produce a good fit to the data. Alternatively, the maximum entropy distributions, as shown in Fig. 4, *D–F*, reveal the two peaks without requiring the assumption of the existence of multiple populations a priori. The information available about probe orientations

in a typical fluorescence polarization experiment is intrinsically limited by the physical nature of absorption and emission. The orientational discrimination of the absorption event is of the form of cosine squared of the angle between the excitation polarization and the probe absorption dipole. Similarly, the orientational discrimination of the fluorescence emission event is given by the cosine squared of the angle between the detector polarizer and the probe emission dipole. Combining the angular discrimination from these two events, terms of up to only the fourth power of the cosine of the probe orientation are accessible. Due to the dipole nature of optical absorption and emission, all of the odd-order (cos, $\cos^3$) terms are also inaccessible. Thus the orientational distribution of a single probe can only be described in terms of $\cos^2$ and $\cos^4$, which are conveniently expressed as the order parameters $\langle P_2 \rangle$ and $\langle P_4 \rangle$ of an expansion (Eq. 1).

The contour maps of Figs. 4, 5, and 7 show more detail about the protein orientational distribution than can be determined from $\langle P_2 \rangle$ and $\langle P_4 \rangle$ of a single probe. However, they also show that the orientational resolution that can be obtained is still limited. With model distributions having more than one domain, the solutions obtained show the two peaks in the appropriate positions, but the technique fails to recover the detailed structure (the relative weights are wrong). Indeed, maximum entropy analysis generally produces the broadest possible distribution consistent with the data, although it will reveal very sharply peaked distributions if forced by the data. The ME distribution reveals the limitations and ambiguities of the experimental data. For example, if the data provide no information about the azimuthal angle of a protein, the maximum entropy distribution will show a flat distribution of azimuthal angles (Figs. 2 *B* and 3 *B*).

Another possibility for combining probe data is to describe the protein orientational distribution by directly determining its order parameters (Ajtai et al., 1992; Van der Heide et al., 1994). To unambiguously define the orientation at second-rank order would require five probe axes, and to define it to fourth-rank order would require a total of nine axes (Zannoni et al., 1983). Because these numbers are impractical, some ambiguity of protein orientation is inevitable. The ME method uses the information available by providing the broadest distribution compatible with the data.

In planning a multiprobe experiment, it is important to make a judicious choice of probe orientations. The simulations illustrating this point here are not exhaustive, because properties of the specific macromolecular system, such as its intrinsic orientation and order in a real experiment, will modify the type of data that are obtained and therefore the available information. The choice of probe positions is limited foremost by accessible labeling sites that do not lead to disruption of the protein's function. Our experiments so far (Hopkins et al., 1997; Corrie et al., 1999) have used pairs of cysteine residues replacing endogenous amino acids. The residues were chosen with 10–15-Å spacing on the surface of the myosin RLC. A relatively clear path in the crystal structure between the two chosen residues was also required. Acceptable bifunctional cross-linking with bis-iodoacetamidorhodamine (Corrie et al., 1998) was shown to occur without compromising the function of the RLC (Corrie et al., 1999). Another promising route to placing probes into protein structures with predetermined orientation is the specific labeling of four engineered cysteines at the i, $i + 1$, $i + 4$, and $i + 5$ positions of an α-helix by bis(dithioarsolanyl)fluorescein (Griffin et al., 1998).

Realizing that the choice of probe orientations is not completely flexible, guidelines are given in Appendix B for evaluating sets of relative probe orientations for their likely evolution of useful data. A figure of merit, M, is derived that indicates the independence of probes in a given set. M is calculated from dot products of vectors based on Wigner rotation matrices, which are orthonormal functions that describe three-dimensional orientational distributions and rotations between frames in spherical coordinates. As an example of the use of M, consider adding successive probe orientations starting with one probe arbitrarily set to axial angle $\theta_1 = 0°$ and azimuthal angle $\phi_1 = 0°$ relative to the protein coordinate frame. A second probe at relative orientation $\theta_2 = 54.7°$ or $\theta_2 = 125.3°$ (irrespective of ϕ_2) will give a value of $M = 1$ for the pair, indicating that the two access independent information. If we now set $\phi_2 = 0$, then, adding a third mutant with ideal orientation $\theta_3 = 54.7°$, $\phi_3 = 68.5°$ yields a set of three mutants, again with $M = 1$. Three other orientations for the third probe also give $M = 1$, $\theta_3 = 54.7°$, $\phi_3 = -68.5°$ and $\theta_3 = 125.3°$, $\phi_3 = \pm 111.5°$. For more than three probes, no set is available with a value $M = 1$. The first four orientations in Set B in Table 1 have a value $M = 0.964$, all 5 have $M = 0.941$. A slightly higher value is obtained when all five orientations are optimized at once rather than added one at a time. In Set B, we successively calculated ideal new orientations given the other ones, because this approach is more similar to a likely experimental program than optimizing five probe orientations from the outset.

In contrast, for a set of two or three perpendicular probe orientations, as given in Table 1 Set 1, $M = 0.75$ indicating overlap in the information provided by the separate probes due to two-fold symmetries of perpendicular dipoles. This overlap results in ambiguity in the maximum entropy distribution recovered from data simulated for these probes (see Results and Fig. 2). Ambiguity of the recovered ME distribution due to such symmetries is avoided when the probe angles are chosen to yield maximal M (Fig. 3).

Probe orientations that maximize M are optimal when no information is available about the protein orientational distribution, but if some experimental data are already at hand, then other criteria may be applicable. For instance, if several probes reveal multiple peaks in an ME distribution, an

additional probe orientation might be selected to verify or rule out one of the peaks. A general design strategy, when there is doubt about the correctness or detail of the ME distribution based on a limited number of probes, is to add probe angles, when possible, that specifically interrogate the uncertain regions of the protein orientational distribution. Thus, the selection of probe orientations, mutation of the protein, labeling studies, validation of protein function, and collection of fluorescence data will most likely be repetitive, but synergistic tasks (Corrie et al., 1999).

The use of bifunctional fluorescent probes has proven to be a powerful experimental tool in obtaining multiple-probe orientations and combining their data (Hopkins et al., 1997; Corrie et al., 1999). Maximum entropy analysis provides a theoretical framework that enables interpretation of data obtained from a set of such probes without the bias of a preselected shape of the distribution. The enhanced angular resolution given by considering data from multiple-probe orientations combined with the method of analysis that can reveal a variety of features in the underlying protein distribution makes fluorescence polarization of bifunctional probes a promising new technique for investigation of structural changes of proteins in larger macromolecular assemblies.

APPENDIX A
THE MAXIMUM ENTROPY DISTRIBUTION

A general derivation of the maximum entropy solution subject to constraints is available in the literature (Jaynes, 1957; Levine and Tribus, 1979). Here, we show the derivation specifically for an orientational distribution function obtained using fluorescence polarization data from n probes. To derive the expression for the ME distribution, we need to maximize the entropy as defined in Eq. 5,

$$S\{f(\beta_{fp}, \gamma_{fp})\} = -\int_0^{\pi}\int_{-\pi}^{\pi} f(\beta_{fp}, \gamma_{fp})\ln\{f(\beta_{fp}, \gamma_{fp})\}\, d\gamma_{fp}\sin\beta_{fp}\, d\beta_{fp}, \quad (A1)$$

by varying the distribution $f(\beta_{fp}, \gamma_{fp})$, under the following constraints:

1. The distribution is positive definite

$$f(\beta_{fp}, \gamma_{fp}) \geq 0. \quad (A2)$$

2. The distribution is normalized

$$\int_0^{\pi}\int_{-\pi}^{\pi} f(\beta_{fp}, \gamma_{fp})\, d\gamma_{fp}\sin\beta_{fp}\, d\beta_{fp} = 1. \quad (A3)$$

3. The distribution must be consistent with the experimentally observed order parameters

$$\langle P_{L,d}(\beta_{fp}, \gamma_{fp})\rangle = \int_0^{\pi}\int_{-\pi}^{\pi} P_{L,d}(\beta_{fp}, \gamma_{fp}) f(\beta_{fp}, \gamma_{fp})\, d\gamma_{fp}\sin\beta_{fp}\, d\beta_{fp}, \quad (A4)$$

where $L = 2, 4$ and $d = 1, 2, \ldots, n$.

For a set of $2n$ independent constraints, we find the maximum entropy distribution subject to these constraints using the method of Lagrange multipliers (Mathews and Walker, 1970). Lagrange found that, if a function S has an extreme value while satisfying the constraints, then the gradient of the function S is a linear combination of the gradients of the constraints. The gradient is taken with respect to the distribution function $f(\beta_{fp}, \gamma_{fp})$. Applied to our case, we find

$$\delta[S\{f(\beta_{fp}, \gamma_{fp})\}] = \delta[(\lambda_0 - 1) + \lambda_{2,d}\langle P_{2,d}(\beta_{fp}, \gamma_{fp})\rangle + \lambda_{4,d}\langle P_{4,d}(\beta_{fp}, \gamma_{fp})\rangle + \cdots]. \quad (A5)$$

Here, the $\lambda_{L,d}$ are called Lagrange multipliers and $d = 1, 2, \ldots, n$. The term -1 in $(\lambda_0 - 1)$ is an offset that will cancel later. Eq. A5 can be rewritten as

$$0 = \delta\int_0^{\pi}\int_{-\pi}^{\pi}\Big\{f(\beta_{fp}, \gamma_{fp})\ln\{f(\beta_{fp}, \gamma_{fp})\} + (\lambda_0 - 1)f(\beta_{fp}, \gamma_{fp}) + \sum_{d=1}^{n}[\lambda_{2,d}P_{2,d}(\beta_{fp}, \gamma_{fp})f(\beta_{fp}, \gamma_{fp}) + \lambda_{4,d}P_{4,d}(\beta_{fp}, \gamma_{fp})f(\beta_{fp}, \gamma_{fp})]\Big\}\, d\gamma_{fp}\sin\beta_{fp}\, d\beta_{fp}. \quad (A6)$$

Using $\delta[f(\beta_{fp}, \gamma_{fp})\ln\{f(\beta_{fp}, \gamma_{fp})\}] = [\ln\{f(\beta_{fp}, \gamma_{fp})\} + 1]\delta f(\beta_{fp}, \gamma_{fp})$, we find

$$0 = \int_0^{\pi}\int_{-\pi}^{\pi}\Big\{\ln\{f(\beta_{fp}, \gamma_{fp})\} + \lambda_0 + \sum_{d=1}^{n}[\lambda_{2,d}P_{2,d}(\beta_{fp}, \gamma_{fp}) + \lambda_{4,d}P_{4,d}(\beta_{fp}, \gamma_{fp})]\Big\}\, d\gamma_{fp}\sin\beta_{fp}\, d\beta_{fp}\delta f(\beta_{fp}, \gamma_{fp}). \quad (A7)$$

This is true if and only if

$$\ln\{f(\beta_{fp}, \gamma_{fp})\} = -\lambda_0 - \sum_{d=1}^{n}[\lambda_{2,d}P_{2,d}(\beta_{fp}, \gamma_{fp}) + \lambda_{4,d}P_{4,d}(\beta_{fp}, \gamma_{fp})]. \quad (A8)$$

Thus,

$$f_{ME}(\beta_{fp}, \gamma_{fp}) = \exp\left\{-\lambda_0 - \sum_{d=1}^{n}[\lambda_{2,d}P_{2,d}(\beta_{fp}, \gamma_{fp}) + \lambda_{4,d}P_{4,d}(\beta_{fp}, \gamma_{fp})]\right\}, \quad \text{(A9)}$$

which is Eq. 6 in the main text.

APPENDIX B
INDEPENDENCE OF PROBE ORIENTATIONS

In this appendix, we use Wigner rotation matrices to derive a parameter, M, that quantifies the degree of independence of information from n probe orientations. In a fluorescence-polarization experiment, intensity ratios are obtained that provide information on the orientational order and rotational dynamics of the transition dipole moments in the system (Lakowicz, 1983; Zannoni, 1983; Kooyman et al., 1983). The orientation distribution of the probe with respect to the sample director **f** can be expressed in terms of the order parameters $\langle P_2(\cos\beta_{fd})\rangle$ and $\langle P_4(\cos\beta_{fd})\rangle$, which represent the second- and fourth-rank Legendre polynomials averaged over the distribution of all dipole orientations β_{fd} (Van Gurp et al., 1988; Van der Heide et al., 1994; Dale et al., 1999; cf., Eq. 1 in the text here). These order parameters can also be expressed in terms of the protein orientation β_{fp}, γ_{fp}, and the orientation of the probe relative to the protein θ_{pd}, ϕ_{pd}. In Eqs. 2 and 3 in the main text, we use the completion theorem to express $\cos\beta_{fd}$ in terms of these angles and substitute this into the equations for calculating the order parameters.

Another approach is to explicitly consider the order parameters that describe the protein orientation distribution. This distribution is conveniently expressed in terms of elements $D^L_{m,n}(\alpha, \beta, \gamma)$ of the Wigner rotation matrix D^L (Rose, 1957). The Wigner functions form an orthonormal set of functions in Euler space defined by the Euler angles α, β, and γ. The elements of rank $L = 2$ used in this appendix are

$$D^L_{m,n}(\alpha, \beta, \gamma) = e^{-im\alpha}d^L_{m,n}(\beta)e^{-in\gamma};$$

$$d^2_{0,0}(\beta) = \tfrac{3}{2}\cos^2(\beta) - \tfrac{1}{2};$$

$$d^2_{1,0}(\beta) = -d^2_{0,1}(\beta) = d^2_{0,-1}(\beta) = -d^2_{-1,0}(\beta) = -\sqrt{\tfrac{3}{2}}\sin(\beta)\cos(\beta); \quad \text{(B1)}$$

and

$$d^2_{2,0}(\beta) = d^2_{0,2}(\beta) = d^2_{0,-2}(\beta) = d^2_{-2,0}(\beta) = \tfrac{1}{2}\sqrt{\tfrac{3}{2}}\sin^2(\beta).$$

When both the axial (β_{fp}) and azimuthal (γ_{fp}) angles are considered, the data provide information about the protein orientation distribution in terms of five second-rank order parameters $\langle D^2_{0,j}(0, \beta_{fp}, \gamma_{fp})\rangle$ (j ranges from -2 to 2) and nine fourth-rank order parameters $\langle D^4_{0,k}(0, \beta_{fp}, \gamma_{fp})\rangle$ (k ranges from -4 to 4) (Rose, 1957; Zannoni, 1983; Van Gurp et al., 1988). In cylindrically symmetrical systems, α_{fp} is not accessible. The relation between these 14 order parameters for the protein orientation distribution and the two order parameters $\langle P_2(\cos\beta_{fd})\rangle$ and $\langle P_4(\cos\beta_{fd})\rangle$ for a probe dipole distribution is found by using the closure relation (Rose, 1957; Zannoni, 1983),

$$\langle P_L(\cos\beta_{fd})\rangle = \sum_{j=-L}^{L}\langle D^L_{0,j}(0, \beta_{fp}, \gamma_{fp})\rangle D^L_{j,0}(\phi_{pd}, \theta_{pd}, 0). \quad \text{(B2)}$$

The order parameters $\langle D^L_{0,j}(0, \beta_{fp}, \gamma_{fp})\rangle$ of the orientational distribution function $f(\beta_{fp}, \gamma_{fp})$, are calculated by averaging the Wigner functions over the orientation distribution, analogous to Eq. 4 in the text.

Depending on the angles θ_{pd}, ϕ_{pd}, each probe constrains certain of the order parameters $\langle D^L_{0,j}(0, \beta_{fp}, \gamma_{fp})\rangle$. To determine all of the second-rank order parameters, five different probe orientations would be required, each providing an independent $\langle P_2(\cos\beta_{fd})\rangle$. For the fourth-rank order parameters, nine further independent probe orientations would be required. Because the most prominent features of the distribution are given by the second rank-order parameters and generating reliable data even from five probe orientations is laborious, the fourth-rank parameters are disregarded for consideration of probe independence in the remainder of this appendix.

To introduce the concept of independence among probes, first take one probe at orientation $\theta_{pd} = 0°$, $\phi_{pd} = 0°$. The definitions of the elements $D^L_{m,n}(\alpha, \beta, \gamma)$ given in Eq. B1 imply that $D^2_{0,0}(0, 0, 0) = 1$, whereas all other second-rank Wigner functions $D^2_{m,n}(0, 0, 0) = 0$. Inserting this information into Eq. B2 gives, in this case, $\langle P_2(\cos\beta_{fd})\rangle_{d=1} = \langle D^2_{0,0}(0, \beta_{fp}, \gamma_{fp})\rangle$. A second probe, oriented at $\theta_{pd} = 54.7°$ (or $\theta_{pd} = 125.3°$) and arbitrary ϕ_{pd}, gives $D^2_{0,0}(54.7°, 0, 0) = 0$, whereas some or all of the other Wigner functions of rank two are nonzero. Thus, in this case, $\langle P_2(\cos\beta_{fd})\rangle_{d=2}$ is not a function of $\langle D^2_{0,0}(0, \beta_{fp}, \gamma_{fp})\rangle$, but depends on the other four second-rank order parameters. This example shows that different probes access different information about the orientational distribution. The information provided by these two probes does not even overlap. An ideal set of probes in combination accesses all of the available order parameters describing $f(\beta_{fp}, \gamma_{fp})$, while having as little overlap as possible.

A practical measure for the interdependence of information accessed by two probes is the inner product of vectors $\mathbf{m}^i$ and $\mathbf{m}^j$, defined as $\mathbf{m}^i_k = D^2_{k,0}(\phi_i, \theta_i, 0)$ and $\mathbf{m}^j_k = D^2_{k,0}(\phi_j, \theta_j, 0)$; k ranges from -2 to $+2$. For a set of n probes with vectors $\mathbf{m}^d$, we define the measure of their independence using the average of all the possible combinations of non-identity inner products

$$M = 1 - \frac{2}{n(n-1)}\sum_{i=1}^{n-1}\sum_{j=i+1}^{n}(\mathbf{m}^i \cdot \mathbf{m}^j), \quad \text{(B3)}$$

where

$$(\mathbf{m}^i \cdot \mathbf{m}^j) \equiv \sum_{k=-2}^{2}(\mathbf{m}^i_k\,\overline{\mathbf{m}^j_k})$$

and $\overline{\mathbf{m}^j}$ is the complex conjugate of $\mathbf{m}^j$. The factor $2/[n(n-1)]$ is used to scale for the number of inner products in the equation. Thus, the value of M ranges from 0 to 1 regardless of the number of probe orientations n. An increasing value of M indicates a greater independence. Values of M are given in the Discussion for the optimal and nonoptimal choices of probe orientations in Table 1 as examples.

We are grateful to Drs. Joe Forkey, Bob Dale, Malcolm Irving, and Henry Shuman for many useful discussions. The work was supported by National Institutes of Health grant AR26846, the Muscular Dystrophy Association and the American Heart Association.

REFERENCES

Ajtai, K., A. Ringler, and T. P. Burghardt. 1992. Probing cross-bridge angular transitions using multiple extrinsic reporter groups. *Biochemistry.* 31:207–217.

Ajtai, K., D. J. Toft, and T. P. Burghardt. 1994. Path and extent of cross-bridge rotation during muscle contraction. *Biochemistry.* 33: 5382–5391.

Bell, M. G., R. E. Dale, U. A. van der Heide, and Y. E. Goldman. 2000. Polarized fluorescence depletion reports orientation distribution and rotational dynamics of muscle crossbridges. *Biophys. J.* 78:120A.

Berger, C. L., J. S. Craik, D. R. Trentham, J. E. T. Corrie, and Y. E. Goldman. 1996. Fluorescence polarization of skeletal muscle fibers labeled with rhodamine isomers on the myosin heavy chain. *Biophys. J.* 71:3330–3343.

Burghardt, T. P., and K. Ajtai. 1992. Mapping global angular transitions of proteins in assemblies using multiple extrinsic reporter groups. *Biochemistry.* 31:200–206.

Burghardt, T. P., and K. Ajtai. 1994. Following the rotational trajectory of the principal hydrodynamic frame of a protein using multiple probes. *Biochemistry.* 33:5376–5381.

Chen, R. F., and R. L. Bowman. 1965. Fluorescence polarization: measurement with ultraviolet-polarizing filters in a spectrophotofluorometer. *Science.* 147:729–732.

Corrie, J. E. T., J. S. Craik, and V. R. N. Munasinghe. 1998. A homobifunctional rhodamine for labeling proteins with defined orientations of a fluorophore. *Bioconjugate Chem.* 9:160–167.

Corrie, J. E. T., B. D. Brandmeier, R. E. Ferguson, D. R. Trentham, J. Kendrick-Jones, S. C. Hopkins, U. A. van der Heide, Y. E. Goldman, C. Sabido-David, R. E. Dale, S. Criddle, and M. Irving. 1999. Dynamic measurement of myosin light-chain-domain tilt and twist in muscle contraction. *Nature.* 400:425–430.

Dale, R. E., S. C. Hopkins, U. A. van der Heide, T. Marszałek, M. Irving, and Y. E. Goldman. 1999. Model-independent analysis of the orientation of fluorescent probes with restricted mobility in muscle fibers. *Biophys. J.* 76:1606–1618.

Dominguez, R., Y. Freyzon, K. M. Trybus, and C. Cohen. 1998. Crystal structure of a vertebrate smooth muscle myosin motor domain and its complex with the essential light chain: visualization of the pre-power stroke state. *Cell.* 94:559–571.

Fajer, P. G. 1994. Determination of spin-label orientation within the myosin head. *Proc. Natl. Acad. Sci. USA.* 91:937–941.

Ferguson, R. E., S. R. Martin, B. D. Brandmeier, J. Kendrick-Jones, R. S. Hodges, B. D. Sykes, J. E. T. Corrie, M. Irving, and D. R. Trentham. 1997. Bifunctional rhodamine-labeled regulatory light chains bind to myosin heavy chains and provide a framework of dipole orientations in fibers. *Biophys. J.* 72:A52.

Griffin, B. A., S. R. Adams, and R. Y. Tsien. 1998. Specific covalent labeling of recombinant protein molecules inside live cells. *Science.* 281:269–272.

Hopkins, S. C., C. Sabido-David, B. D. Brandmeier, J. Kendrick-Jones, R. E. Dale, J. E. T. Corrie, D. R. Trentham, M. Irving, and Y. E. Goldman. 1997. Motions of bifunctional rhodamine probes with defined orientations on the regulatory light chain (RLC) in skeletal muscle fibers. *Biophys. J.* 72:A1.

Hopkins, S. C., C. Sabido-David, J. E. T. Corrie, M. Irving, and Y. E. Goldman. 1998. Fluorescence polarization transients from rhodamine isomers on the myosin regulatory light chain in skeletal muscle fibers. *Biophys. J.* 74:3093–3110.

Irving, M., T. St. C. Allen, C. Sabido-David, J. S. Craik, B. Brandmeier, J. Kendrick-Jones, J. E. T. Corrie, D. R. Trentham, and Y. E. Goldman. 1995. Tilting of the light-chain region of myosin during step length changes and active force generation in skeletal muscle. *Nature.* 375: 688–691.

Jaynes, E. T. 1957. Information theory and statistical mechanics. *Phys. Rev.* 106:620–630.

Kinosita, K., Jr., S. Kawato, and A. Ikegami. 1977. A theory of fluorescence polarization decay in membranes. *Biophys. J.* 20:289–305.

Kooyman, R. P. H., M. H. Vos, and Y. K. Levine. 1983. Determination of orientational order parameters in oriented lipid membrane systems by angle-resolved fluorescence depolarization experiments. *Chem. Phys.* 81:461–472.

Lakowicz, J. R. 1983. Principles of Fluorescence Spectroscopy. Plenum Press, New York. 111–153.

Levine, R. D., and M. Tribus. 1979. The Maximum Entropy Formalism. M.I.T. Press, Cambridge, MA. 1–14.

Mathews, J., and R. L. Walker. 1970. Mathematical Methods of Physics, 2nd ed. The Benjamin/Cummings Publishing Company, Reading, MA. 327–333.

Mchaourab, H. S., M. A. Lietzow, K. Hideg, and W. L. Hubbell. 1996. Motion of spin-labeled side chains in T4 lysozyme. Correlation with protein structure and dynamics. *Biochemistry.* 35:7692–7704.

Polekhina, G., S. Thirup, M. Kjeldgaard, P. Nissen, C. Lippmann, and J. Nyborg. 1996. Helix unwinding in the effector region of elongation factor EF-Tu-GDP. *Structure.* 4:1141–1151.

Press, W. H., S. A. Teukolsky, W. T. Vetterling, and B. P. Flannery. 1992. Numerical Recipes in C: The Art of Scientific Computing. Cambridge University Press, New York. 804–826.

Rose, M. E. 1957. Elementary Theory of Angular Momentum. Wiley, New York.

Sabido-David, C., R. E. Ferguson, B. D. Brandmeier, S. C. Hopkins, Y. E. Goldman, J. Kendrick-Jones, R. E. Dale, J. E. T. Corrie, D. R. Trentham, and M. Irving. 1997. Orientation of bifunctional rhodamine probes on myosin regulatory light chain (RLC) in relaxed, contracting and rigor muscle. *Biophys. J.* 72:A52.

Shannon, C. E. 1948. A mathematical theory of communication. *Bell Syst. Tech. J.* 27:379–423.

Smith, W. J. 1990. Modern Optical Engineering: The Design of Optical Systems, 2nd ed. McGraw-Hill, New York. 152–153.

Van der Heide, U. A., S. C. Hopkins, and Y. E. Goldman. 1998. A maximum entropy analysis of the orientation of regulatory light chains in skeletal muscle fibers. *Biophys. J.* 74:A364.

Van der Heide, U. A., B. Orbons, H. C. Gerritsen, and Y. K. Levine. 1992. The orientation of transition moments of dye molecules used in fluorescence studies of muscle systems. *Eur. Biophys. J.* 21:263–272.

Van der Heide, U. A., O. E. Rem, H. C. Gerritsen, E. L. de Beer, P. Schiereck, I. P. Trayer, and Y. K. Levine. 1994. A fluorescence depolarization study of the orientational distribution of crossbridges in muscle fibers. *Eur. Biophys. J.* 23:369–378.

VanderMeulen, D. L., D. G. Nealon, E. Gratton, and D. M. Jameson. 1990. Excitation wavelength dependent fluorescence anisotropy of eosin-myosin adducts. *Biophys. Chem.* 36:177–184.

Van Gurp, M., H. van Langen, G. van Ginkel, and Y. K. Levine. 1988. Angle-resolved techniques in studies of organic molecules in ordered systems using polarized light. *In* Polarized Spectroscopy of Ordered Systems. B. Samori' and E. W. Thulstrup, editors. Kluwer Academic Publishers, Boston, MA. 455–489.

Weber, G. 1952. Polarization of the fluorescence of macromolecules. 1. Theory and experimental method. *Biochemistry.* 51:145–155.

Wilson, M. G. A., and R. A. Mendelson. 1983. A comparison of order and orientation of crossbridges in rigor and relaxed muscle fibres using fluorescence polarization. *J. Muscle Res. Cell Motil.* 4:671–693.

Yasuda, R., H. Noji, K. Kinosita, Jr., and M. Yoshida. 1998. F_1-ATPase is a highly efficient molecular motor that rotates with discrete 120° steps. *Cell.* 93:1117–1124.

Zannoni, C. 1988. Order parameters and orientational distributions in liquid crystals. *In* Polarized Spectroscopy of Ordered Systems. B. Samori' and E. W. Thulstrup, editors. Kluwer Academic Publishers, Boston, MA. 57–83.

Zannoni, C., A. Arcioni, and P. Cavatorta. 1983. Fluorescence depolarization in liquid crystals and membrane bilayers. *Chem. Phys. Lipids.* 32:179–250.

Zhang, Z., L. Huang, V. M. Shulmeister, Y.-I. Chi, K. K. Kim, L.-W. Hung, A. R. Crofts, E. A. Berry, and S.-H. Kim. 1998. Electron transfer by domain movement in cytochrome bc_1. *Nature.* 392:677–684.